nature immunology

Direct priming of antiviral CD8+ T cells in the peripheral interfollicular region of lymph nodes

Heather D Hickman[1], Kazuyo Takeda[1], Cara N Skon[1], Faith R Murray[1], Scott E Hensley[1], Joshua Loomis[2], Glen N Barber[2], Jack R Bennink[1] & Jonathan W Yewdell[1]

It is uncertain how antiviral lymphocytes are activated in draining lymph nodes, the site where adaptive immune responses are initiated. Here, using intravital microscopy we show that after infection of mice with vaccinia virus (a large DNA virus) or vesicular stomatitis virus (a small RNA virus), virions drained to the lymph node and infected cells residing just beneath the subcapsular sinus. Naive CD8+ T cells rapidly migrated to infected cells in the peripheral interfollicular region and then formed tight interactions with dendritic cells, leading to complete T cell activation. Thus, antigen presentation at the lymph node periphery, not at lymphocyte exit sites in deeper lymph node venules, as dogma dictates, has a dominant function in antiviral CD8+ T cell activation.

The primary adaptive immune response to most pathogens and vaccines is initiated in regional lymph nodes draining peripheral sites of antigen exposure. Lymph nodes are highly organized structures designed to efficiently transfer antigen transported from the periphery to node-resident cells specialized in acquiring, processing and presenting antigen to lymphocytes. Lymphatics deliver lymph-borne antigens to the lymph node subcapsular sinus (SCS), where antigen can be collected by cells lining the sinus. Antigens can also travel through the lymph node via specialized conduits, traversing many cell types before eventually exiting the node through the efferent lymphatic vessel[1,2]. Additional viral antigen is potentially delivered later to the lymph node in the context of antigen-laden cells migrating into the node after peripheral maturation.

The application of multiphoton-based intravital microscopy (IVM) has deepened the understanding of immune response initiation, particularly the central issues of when and where naive, antigen-specific lymphocytes encounter cognate antigen-presenting cells (APCs) in the lymph node[3–6]. Initial IVM studies showed that adoptively transferred fluorescence-labeled naive T cells and B cells enter the lymph node through high endothelial venules (HEVs), scan HEV-associated dendritic cells (DCs) and form stable conjugates in an antigen-specific way, leading to lymphocyte activation[7–10]. This model uses adoptive transfer of peptide-pulsed, *in vitro*–propagated DCs, and its relevance to viral infection and other physiologic situations remains to be established. Indeed, studies have shown that B cells encounter cognate lymph node-draining antigen just beneath the SCS rather than near HEVs[11–13]. Here we sought to determine if antiviral CD8+ T cells encounter antigen similarly.

RESULTS

Visualization of virus-infected cells under the SCS

To address the issue of how antiviral CD8+ T cells encounter antigen, we developed a model system in which mice are infected with vaccinia virus (VV) or vesicular stomatitis virus (VSV) in the flank and the draining inguinal lymph node (ILN) is imaged in anesthetized mice by IVM. VV is a double-stranded DNA virus with a genome of 200 kilobases encoding over 250 open reading frames. VSV is a negative-stranded RNA virus with an 11-kilobase genome encoding only five open reading frames. For each of these, we infected mice with recombinant virus expressing enhanced green fluorescent protein (eGFP) genetically fused to influenza nucleoprotein (NP) with the model H-2K^b-restricted peptide SIINFEKL sandwiched between them (NP-S-eGFP)[14]. This nucleoprotein is karyophilic, making it easy to distinguish infected cells (through its nuclear fluorescence pattern) from cells that have acquired NP-S-eGFP from other cells (through its endosomal-phagosomal fluorescence pattern). Notably, infected cells could be easily visualized in draining ILNs within 2–3 h of inoculation (**Fig. 1a**,**b**). Because NP-S-eGFP expression occured on the same time scale noted when virus was simply added to cells *in vitro*, this indicated that many infectious virions rapidly transited the lymphatics and arrived at susceptible cells in the ILN probably within minutes. Even at the earliest time points assessed after injection, we detected many infected cells (up to 1,700 per *xyz* field of 750 μm × 750 μm × 20 μm). For each virus, the number of infected cells (and intensity of eGFP) peaked between 6 h and 9 h, remained steady until 12–14 h after infection, and then gradually decreased over the next 24 h (**Fig. 1a**,**b**).

[1]Laboratory of Viral Diseases, National Institute of Allergy and Infectious Diseases, Bethesda, Maryland 20892, USA. [2]Department of Microbiology and Immunology and Sylvester Comprehensive Cancer Center, University of Miami School of Medicine, Miami, Florida 33136, USA. Correspondence should be addressed to J.W.Y. (jyewdell@mail.nih.gov).

Received 18 September 2007; accepted 11 December 2007; published online 13 January 2008; doi:10.1038/ni1557

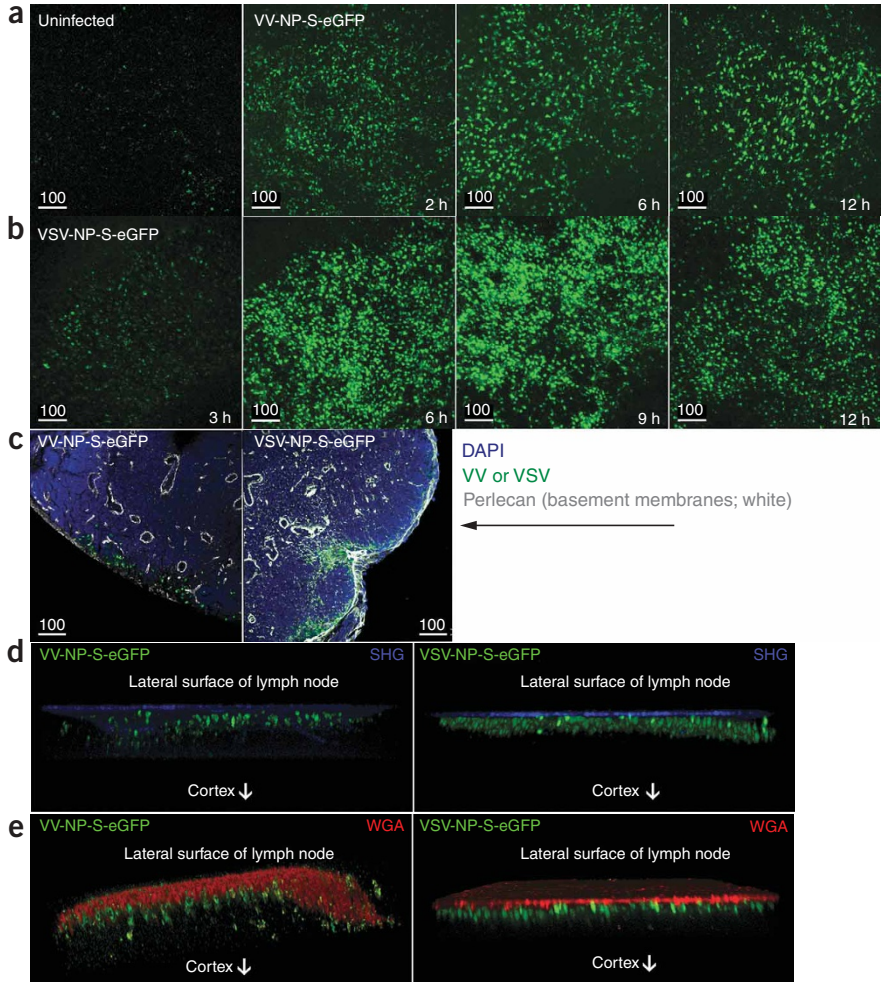

Figure 1 Cells infected with VV and VSV are located just beneath the SCS. (**a**,**b**) Multiphoton IVM of cells in the ILNs of mice left uninfected or infected subcutaneously in the flank with approximately 3.5×10^7 PFU VV-NP-S-eGFP (green nuclear staining; **a**) or 4×10^7 PFU VSV-NP-S-eGFP (green nuclear staining; **b**); images were acquired 2–12 h after injection (time, bottom right corner). (**c**) Frozen section of a VV-infected ILN (left, green) or VSV-infected ILN (right, green) at 10 h after infection, stained with DAPI (blue; 4,6-diamidino-2-phenylindole) and anti-perlecan (white) to show basement membranes (including the floor of the SCS). (**d**,**e**) Three-dimensional reconstruction of an infected (green) ILN visualized with IVM. (**d**) Collagen fibers (blue) visualized by second-harmonic generation (SHG) 6–8 h after infection with VV (left) or VSV (right). (**e**) Identification of SCS macrophages with rhodamine wheat germ agglutinin (WGA; red) given subcutaneously after infection with VV (left) or VSV (right). Scale bars, μm. Related images, **Supplementary Video 1**. All experiments were repeated independently two to four times.

IVM showed that most virus-infected cells resided in a nearly continuous sheet at the lymph node periphery. Staining of the basement membranes of frozen lymph node sections 12 h after infection showed that the infected cell layer was just below the SCS floor (**Fig. 1c**). IVM confirmed that this layer was located below the lymph node capsule (visualized by excitation of collagen fluorescence; **Fig. 1d**) and just beneath the SCS (visualized by staining with fluorescent wheat germ agglutinin[15]; **Fig. 1e**). Infected cells in this area were mostly nonmotile, with an average speed of 1.56 μm/min or 1.53 μm/min for VV or VSV, respectively (**Supplementary Fig. 1** and **Video 1** online). With either virus, a few infected cells moved at higher speed and may have represented a distinct cell type in this anatomic region.

CD8$^+$ T cells relocate in close proximity to virus-infected cells

Although virus-infected cells were located almost exclusively at the periphery of the lymph node here, microscopy studies have shown that CD8$^+$ T cells enter uninfected lymph nodes in a deeper area (through HEVs in the outer paracortex), moving centripetally into the T cell area, which fans out beneath B cell follicles[16,17]. Notably, in uninfected mice, CD8α$^+$ DCs are found in this region, and these cells have been suggested by *ex vivo* studies to be the only lymph node cell type capable of priming CD8$^+$ T cells after VV infection[18,19]. Additionally, many studies have visualized interactions of T cells with immigrant antigen-bearing DCs in the lymph node paracortex adjacent to HEVs in this region[9,17,20,21]. It was therefore unexpected that adoptively transferred T cell receptor–transgenic OT-I CD8$^+$ T cells (specific for H-2K^b SIINFEKL) did not localize mainly to this region after VV or VSV infection (**Fig. 2**).

We first visualized the distribution of OT-I cells in relation to the SCS (with fluorescein-conjugated wheat germ agglutinin) in uninfected mice. Consistent with earlier IVM studies[22,23], in uninfected ILNs, most OT-I cells were located centrally in the T cell zone underlying B cell follicles (**Fig. 2a** and **Supplementary Video 2** online). However, after infection with VV-NP-S-eGFP or VSV-NP-S-eGFP, OT-I cells relocated to the peripheral regions of the lymph node (**Fig. 2b**,**c**) near the SCS and formed contacts with infected cells. Examination of ILNs at earlier times after infection showed that OT-I cells localized to the lymph node periphery soon after NP-S-eGFP expression could be detected in the peri-SCS region. In many cases, we noted OT-I cell redistribution as early as 2–3 h after infection (**Fig. 2d**,**e**). After redistribution, OT-I cells formed contacts with infected cells in the region. In most cases, the redistribution was complete (few CD8$^+$ T cells noted in the deep cortex beneath the imaging area) by 6 h after infection. We assessed the persistence of peripheral relocation of CD8$^+$ T cells in the ILNs by transferring OT-I cells at increasing intervals after VV infection (**Fig. 2f**). OT-I cells entered nodes and migrated peripherally for as long as infected cells were detected under the lymph node SCS, although over time, the number of relocated OT-I cells waned as a function of the number of infected cells. By 42 h after infection, few VV-infected cells were detected in the ILNs, and OT-I cell relocation had mostly ceased.

CD8$^+$ T cells relocate to the peri-SCS

The peri-SCS region that attracts CD8$^+$ T cells after infection is superficial to HEV-laden zones in the lymph node paracortex[17,24]. To more precisely establish the relationship (if any) between CD8$^+$ T cell–infected cell conjugates and HEVs, we visualized HEVs by injecting a fluorescein isothiocyanate (FITC)–conjugated HEV-specific monoclonal antibody (**Fig. 3a**). At 6 h after infection

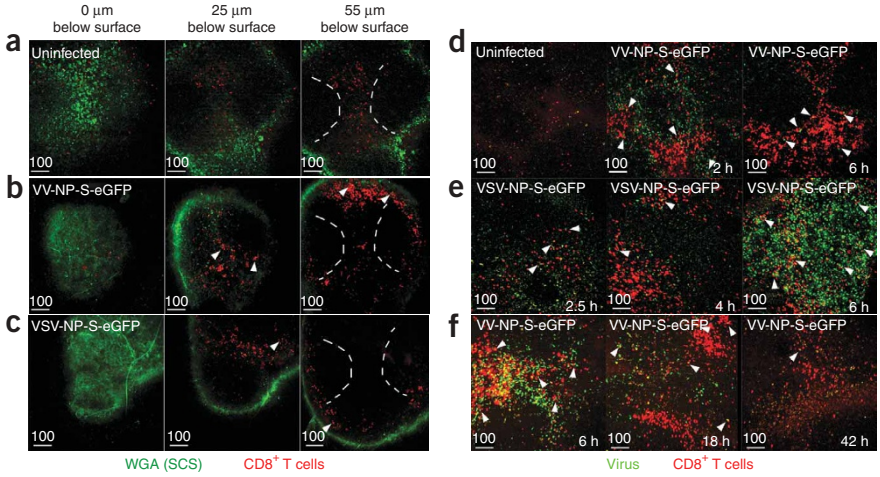

Figure 2 CD8$^+$ T cells redistribute after infection with VV or VSV. (**a**–**c**) IVM of the relocation of OT-I cells (red) in mice given 1.0×10^7 to 1.5×10^7 OT-I cells 12 h before being infected with 3.5×10^7 PFU of VV-NP-S-eGFP or 4×10^7 PFU of VSV-NP-S-eGFP (bright green nuclear staining); FITC–wheat germ agglutinin (more diffuse green staining) was given 30 min before imaging for identification of the SCS, and images were obtained 6 h after infection. Individual 5-μm sections of the ILN are presented from the outer surface (left), or 25 μm (middle) or 55 μm (right) beneath the SCS. Dashed white lines (right) delineate the T cell zone underlying B cell follicles; arrowheads (**b**,**c**) indicate representative contacts formed with infected cells. (**a**) Uninfected ILN. (**b**) ILN infected with VV. (**c**) ILN infected with VSV. (**d**,**e**) Timing of the relocation of OT-I cells (red) in mice left uninfected or infected with VV-NP-S-eGFP (green; **d**) or VSV-NP-S-eGFP (green; **e**). (**f**) IVM of the time course of relocation of OT-I cells in mice infected with VV-NP-S-eGFP for 0, 12 or 36 h before transfer of 1.5×10^7 OT-I cells (red). In **d**–**f**, images acquired 2–6 h (**d**,**e**) or 6–42 h (**f**) after infection (time, bottom right corner) are presented as three-dimensional projections of the top 40 μm of the ILN. Arrowheads indicate contacts formed between OT-I cells and infected cells after redistribution. Scale bars, μm. Related images, **Supplementary Video 2**. All results are representative of at least three independent experiments.

with VV-SIINFEKL (expressing SIINFEKL peptide as a cytosolic 'minigene' product), OT-I cell clusters were located more superficially than the outermost HEVs. To further spatially relate HEV location to cluster-formation sites, we intravenously injected OT-I cells together with fluorescein-dextran into mice infected with VV-NP-S-eGFP (**Fig. 3b** and **Supplementary Video 3** online). OT-I cells entered the ILNs through multiple distinct points along HEVs (as shown on vessels filled with fluorescein-dextran); these entry points were obviously deeper than the layer of infected cells. Fluorescein-dextran leaked slightly from blood vessels, resulting in the uptake of dye by SCS macrophages (**Fig. 3b**, left and middle left). For a less obstructed view of infected cells, we repeated the experiment without fluorescein-dextran (**Fig. 3c**). Over an extended imaging period (approximately 4 h after transfer), we imaged OT-I cells entering the T cell paracortex through the HEVs and moving centrifugally to interact with cells at the periphery of the ILN (**Fig. 3d**). Confirming those findings, we analyzed frozen sections of ILNs containing OT-I cells and F5 cells (T cell receptor–transgenic CD8$^+$ T cells specific for H-2D^b–ASNENMDAM complexes) at 12 h after infection with VV-OVA (expressing SIINFEKL; **Fig. 3e**). This showed that F5 cells remained in the central T regions containing HEVs (stained after sectioning), whereas OT-I cells migrated to the peri-SCS area.

Although CD8$^+$ T cell–infected cell conjugates were physically distinct from HEVs, accumulation of antigen-specific CD8$^+$ T cells could possibly have resulted from the migration of cells across the short distance from the most peripheral HEVs as they entered the lymph node (**Fig. 3e**, HEV example), whereas non–antigen-specific

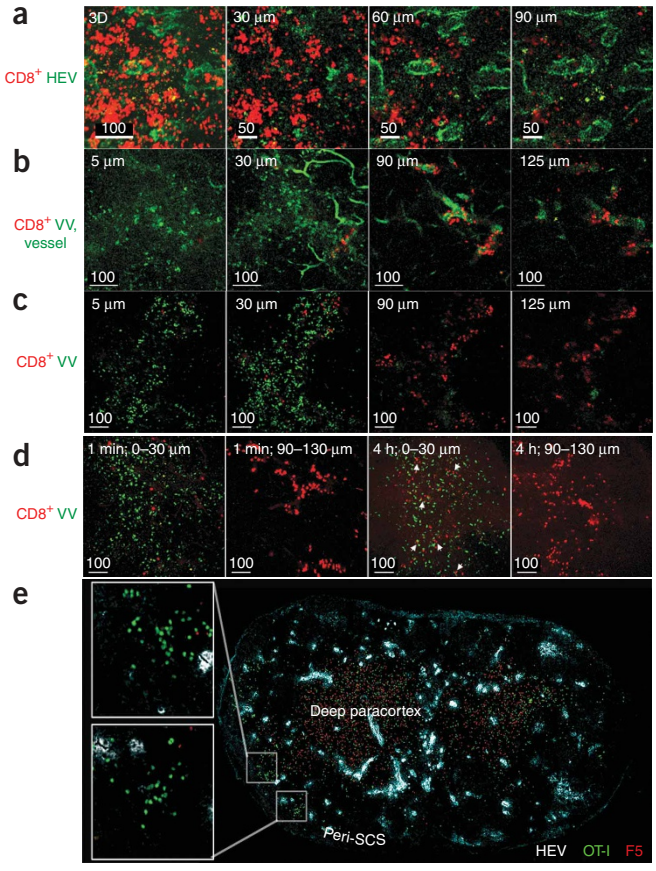

Figure 3 CD8$^+$ T cells cluster peripherally from the HEVs and deep paracortex. (**a**) Three-dimensional (3D) projection of a 165-μm section of an infected ILN, or single sections collected at depths of 30, 60, or 90 μm (top left corner) below the SCS, in mice given 1.5×10^7 OT-I cells (red) 12 h before infection with VV-SIINFEKL (nonfluorescent); 6 h after infection, HEVs were visualized by intravenous injection of FITC-conjugated monoclonal anti-HEV (green). (**b**,**c**) IVM of cells from mice infected with VV-NP-S-eGFP (green, nuclear staining) for 6 h before intravenous injection of 1.5×10^7 OT-I cells (red) with (**b**) or without (**c**) Fluorescein-dextran to indicate vasculature (green; vessel localized); images were obtained 1 min after cell transfer. (**d**) ILN imaged continuously for 4 h after injection of OT-I cells as described in **b**. Left, three-dimensional projections of the ILN from μm beneath the SCS (far left) or from 90-130 μm deep (middle left); right, same ILN 4 h after transfer. White arrowheads indicate OT-I cells that moved into the peri-SCS area (0–30 μm deep). (**e**) Cross-section of an entire ILN at 12 h after infection with VV-SIINFEKL (nonfluorescent), assembled from standard confocal images of a 30-μM cryosection. OT-I cells (green) and F5 cells (red) were transferred before infection; HEVs are cyan. Scale bars, μm. Related images, **Supplementary Videos 3** and **4**. All results are representative of at least three independent experiments.

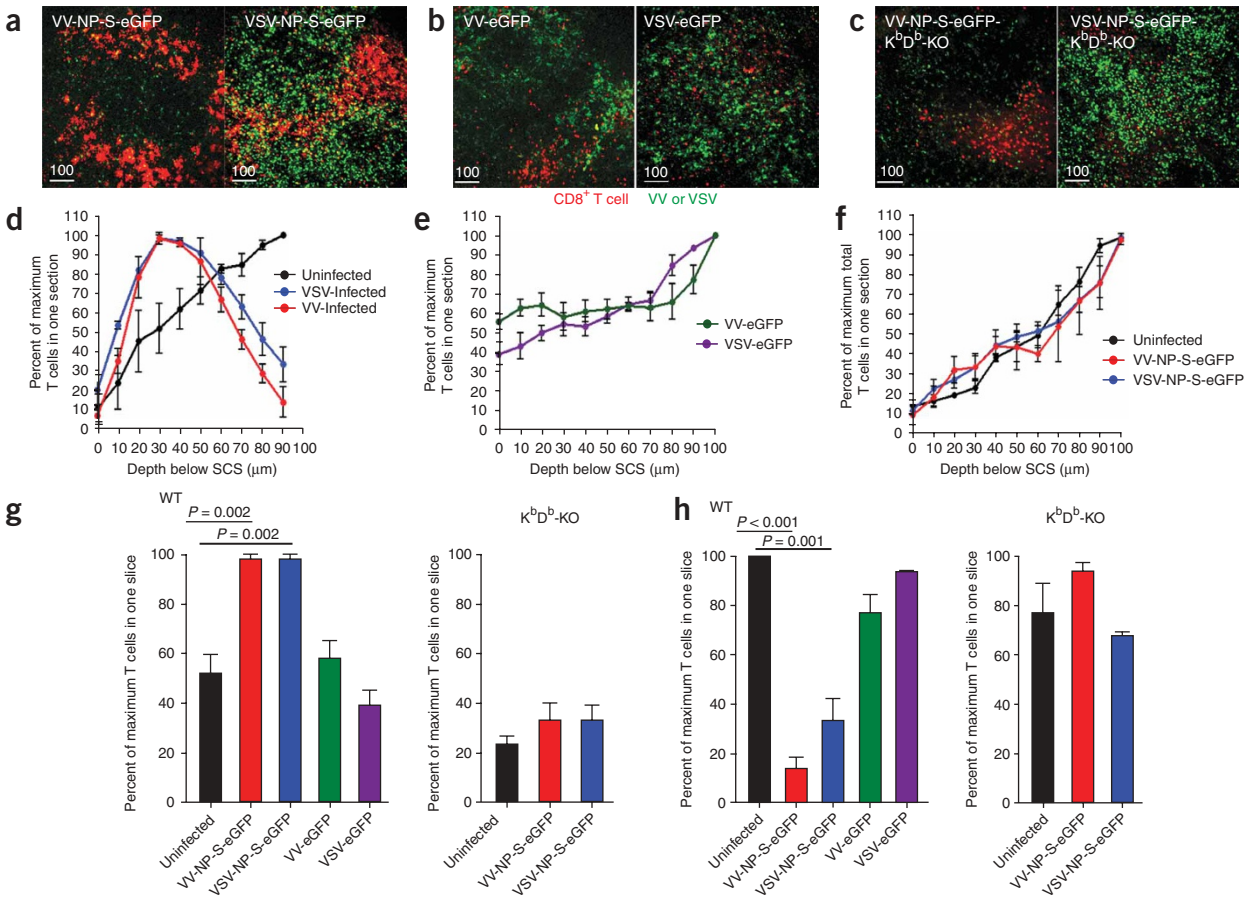

Figure 4 CD8$^+$ T cell redistribution requires antigen. Analysis of OT-I cell density and distance beneath the SCS in wild-type mice (WT) or mice with targeted deletion of H-2K^{b}H-2D^b (K^{b}D^b-KO) given 1.5×10^7 OT-I cells (red) before infection with VV or VSV (green); images were acquired 6 h after infection. (**a**–**c**) Three-dimensional reconstruction of the ILN. (**a**) Wild-type mice infected with VV-NP-S-eGFP (left) or VSV-NP-S-eGFP (right). (**b**) Wild-type mice infected with VV-eGFP (left) or VSV-eGFP (right) lacking SIINFEKL. (**c**) Mice with targeted deletion of H-2K^{b}H-2D^b, infected with VV-NP-S-eGFP (left) or VSV-NP-S-eGFP (right). Scale bars, μm. (**d**–**f**) Percent OT-I cells in a given section, normalized to the maximum number of T cells in one section of an ILN. Results are representative of three mice per group. (**d**) Wild-type mice left uninfected or infected with VV-NP-S-eGFP or VSV-NP-S-eGFP. (**e**) Wild-type mice infected with VV-eGFP or VSV-eGFP. (**f**) Mice with targeted deletion of H-2K^{b}H-2D^b, left uninfected or infected with VV-NP-S-eGFP or VSV-NP-S-eGFP. (**g**,**h**) Percent OT-I cells located 30 μm (**g**) or 90 μm (**h**) under the SCS in mice infected with various VVs or VSVs (horizontal axes). Statistical analyses, unpaired *t*-test. All experiments were repeated at least three independent times (error bars, s.e.m.).

T cells continued centripetally as usual into the inner paracortex. Alternatively, antigen-specific CD8$^+$ T cells already present in the inner paracortex at the time of infection could have relocated to the peri-SCS area. To examine those possibilities, we blocked entry of CD8$^+$ T cells into the ILN as described before[9] by administering antibody to CD62L (anti-CD62L) 12 h before infection (**Supplementary Fig. 2** online). Cluster formation was not inhibited by anti-CD62L, which showed that OT-I cells that had migrated to the node in the 12-hour period before the blockade relocated from the deeper T cell zone to the peri-SCS area after infection of lymph nodes with VV. When we gave OT-I cells concomitantly with virus infection so we visualized only newly lymph node–entrant CD8$^+$ T cells, we also saw redistribution to the peri-SCS region (**Supplementary Fig. 2** and **Video 4** online). Thus, both mechanisms probably contributed to the redistribution of OT-I cells to the peri-SCS area.

Cognate antigen–driven centrifugal relocation of CD8$^+$ T cells

To determine the mechanism underlying CD8$^+$ T cell redistribution and speed reduction at the periphery, we measured the density of OT-I cells relative to their distance beneath the SCS in various conditions (**Fig. 4**). First, we visualized OT-I CD8$^+$ T cells in the ILNs of uninfected wild-type mice or from 6 h to 10 h after infection with VV-NP-S-eGFP or VSV-NP-S-eGFP (**Fig. 4a**) and calculated the density of OT-I cells at increasing depths in the ILN (**Fig. 4d**). As expected from prior studies[17], OT-I cells in uninfected ILNs were concentrated in the inner paracortex of the T cell zone (approximately 90 μm below the SCS). In both the VV- and VSV-infected ILNs, however, OT-I cell density was maximum just 30 μm beneath the SCS, where OT-I cells were located nearly exclusively in the interfollicular region. The difference in the percent of OT-I cells located 30 μm (**Fig. 4g**) or 90 μm (**Fig. 4h**) beneath the SCS was statistically significant after infection with either VV or VSV.

We next analyzed the requirement for cognate antigen in CD8$^+$ T cell relocation by infecting mice with either VV or VSV expressing eGFP lacking SIINKFEKL (**Fig. 4b**). After infection with virus lacking cognate peptide, CD8$^+$ T cells were more evenly distributed throughout the ILN (although this difference was not statistically significant), which indicated that infection alone induced partial centrifugal relocation of CD8$^+$ T cells (**Fig. 4e**). We also similarly infected mice with a targeted deletion of the H-2K^{b}H-2D^b genes (**Fig. 4c**). In the

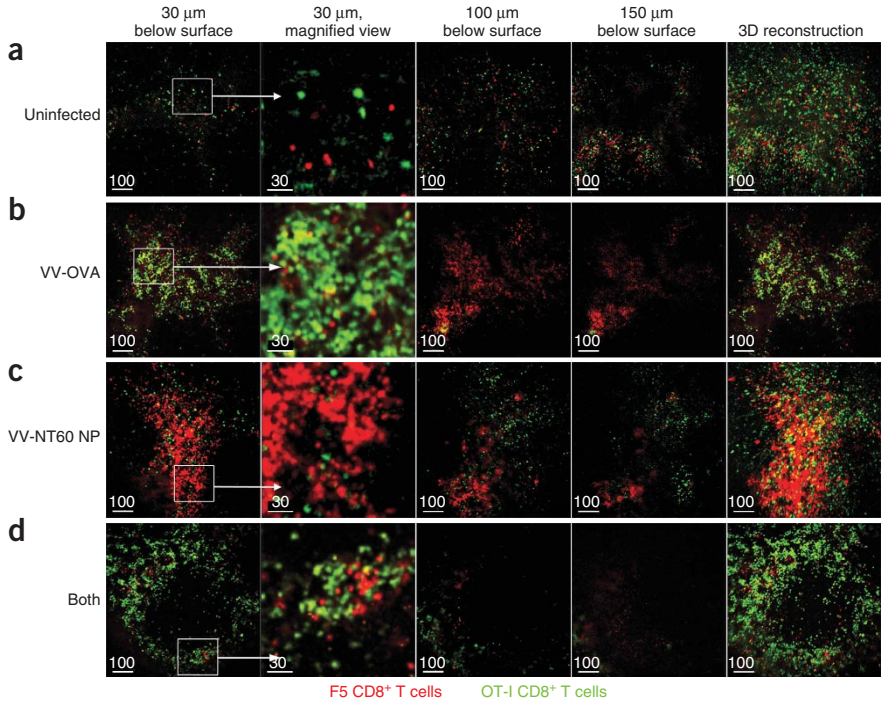

Figure 5 Only antigen-specific CD8$^+$ T cells accumulate at the periphery. IVM of ILNs from mice given 1.5×10^7 OT-I cells (green) and F5 cells (red), then left uninfected (**a**) or infected 12 h later with VV-OVA (**b**), VV-NT60 NP (**c**) or both viruses (**d**) and imaged 6–10 h after infection. Individual 5-μm sections were obtained at a depth of 30, 100 or 150 μm beneath the ILN surface. Outlined area of each 30-μm section at far left is magnified in the adjacent panel; far right, three-dimensional projection. VV-OVA encodes SIINFEKL; VV-NT60 NP encodes ASNENMDAM. Scale bars, μm. Related images, **Supplementary Video 6**. All experiments were repeated at least four independent times.

absence of cognate major histocompatibility complex (MHC) class I molecules, there was no substantial redistribution of OT-I cells to the node periphery after infection with either virus expressing NP-S-eGFP (**Fig. 4f**). These findings collectively demonstrate that viral infection alone results in limited centrifugal redistribution of CD8$^+$ T cells in an MHC class I–dependent way, whereas full-scale redistribution requires the cognate MHC class I peptide complex.

In further experiments we used T cell receptor–transgenic CD8$^+$ T cells with various distinct specificities to assess the requirement for cognate antigen in the redistribution of CD8$^+$ T cells to the lymph node periphery (**Fig. 5**). We transferred OT-I cells together with F5 cells into mice that we later infected with a nonfluorescent VV expressing an antigen containing peptide(s) recognized by OT-I cells, F5 cells, or both CD8$^+$ T cell clones (**Fig. 5b–d** and **Supplementary Video 5** online). In uninfected mice, the two clones were similarly distributed in the ILN (**Fig. 5a**). VV expression of cognate antigen resulted in specific accumulation of the corresponding CD8$^+$ T cell clone at the lymph node periphery, whereas the nonspecific CD8$^+$ T cell clone remained in the deeper T cell zone. Simultaneous presentation of both cognate complexes resulted in redistribution of the two CD8$^+$ T cell clones together. This experiment establishes that CD8$^+$ T cell redistribution is highly dependent on the interaction of individual CD8$^+$ T cells with APCs bearing cognate antigen and not on general CD8$^+$ T cell migration after infection (which is limited).

Long-lasting CD8$^+$ T cell contacts after viral infection

To determine if relocation to the ILN periphery was accompanied by alterations in OT-I cell mobility, we calculated the speed of OT-I cells after viral infection of the draining lymph node (**Supplementary Fig. 3** online). In uninfected ILNs, we noted an average speed of OT-I cells (10.8 μm/min) similar to values reported before[7,9]. After VV infection, the mobility of CD8$^+$ T cells varied with the time after infection, the number of CD8$^+$ T cells transferred, the number of infected cells present and CD8$^+$ T cell depth in the lymph node. For example, in heavily infected lymph nodes, nearly all of the OT-I cells relocated to the periphery and the average speed of CD8$^+$ T cells reflected only the relocated cells. To more accurately measure CD8$^+$ T cell speed during their centrifugal relocation, we infected mice with one fifth the amount of VV we typically used, which resulted in fewer infected cells and incomplete relocation of OT-I cells to the periphery. We then calculated the speed of OT-I cells at 6 h after infection in distinct 5-μm sections, beginning from the most peripheral region containing VV-infected cells (**Supplementary Fig. 3** and **Video 6** online). Peripheral OT-I cells moved much more slowly, with an average speed of 2.86 μm/min, slowing to speeds near those of infected cells. Notably, some peripheral CD8$^+$ T cells maintained a high speed. OT-I cells gradually increased their speed proportional to their distance from the periphery, until they attained speeds near those found deep in the cortex of uninfected mice (10.6 μm/min). Likewise, the distance individual OT-I cells traveled during a given imaging period increased with increasing lymph node depth. The decrease in mobility corresponding with intranodal location was most evident when we plotted the tracks of OT-I cells in 5-μm sections along with the individual displacement of CD8$^+$ T cells from their starting points.

The accumulation of OT-I cells at the lymph node periphery probably involved long-lasting interactions between CD8$^+$ T cells and virus-infected cells. We examined these contacts with higher-resolution imaging of a 40-μm area in the peri-SCS (**Supplementary Figs. 4–6** online). Consistent with their redistribution patterns, the interactions of OT-I cells with infected cells were controlled by the presence of antigenic ligands. When APCs presented H-2K^b-SIINFEKL complexes, OT-I cells formed tight, persistent contacts with cells expressing NP-S-eGFP (**Supplementary Figs. 4,5** and **Videos 7,8** online), even moving if necessary to maintain contact with the rare mobile infected cell (**Supplementary Video 9** online). Such contacts can probably last many hours, as we only infrequently noted conjugate dissociation during 45-minute imaging periods (**Supplementary Fig. 6**). When APCs expressed H-2K^b but not SIINFEKL, OT-I cells formed transient contacts. In the absence of H-2K^b (and H-2D^b) molecules, we failed to detect contact between OT-I cells and infected cells (**Supplementary Figs. 4,5**). Thus, MHC class I expression is required for the formation of transient contacts between infected cells and OT-I cells, with more stable interactions requiring expression of a cognate H-2K^b-SIINFEKL complex.

CD8$^+$ T cells rapidly contact infected APCs

We next determined the identity of the APCs that nucleated CD8$^+$ T cells clusters. As reported before[14], most VV-infected cells in

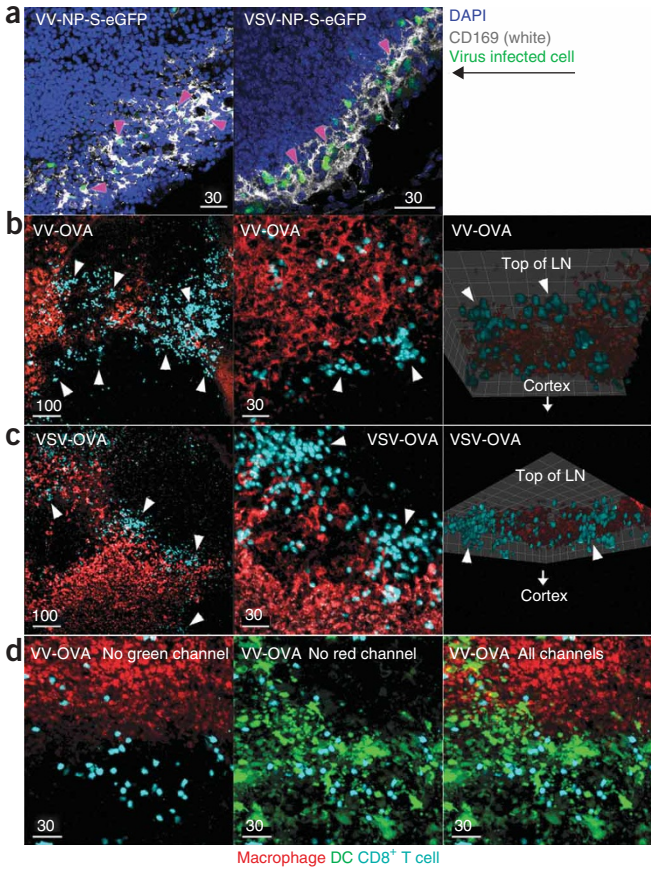

Figure 6 CD8$^+$ T cells cluster with DCs outside the macrophage-rich area. (**a**) Frozen section of a VV-infected ILN (left; green) or VSV-infected ILN (right; green) stained with DAPI (blue) and anti-CD169 (white) to show infected CD169$^+$ macrophages. Magenta arrowheads indicate some of the CD169$^+$ infected cells. (**b**,**c**) IVMs of ILNs from mice given 1.5×10^7 OT-I cells ('pseudocolored' blue) and infected with VV-OVA (**b**) or VSV-OVA (**c**); at 8–10 h after infection, mice were given fluorescent dextran subcutaneously to label macrophages (red) and were imaged 30 min later. Images are three-dimensional reconstructions of a 20× view (left), a 63× view (middle) and a view of the middle image turned on the side (right). Arrowheads indicate clusters outside the macrophage zone. (**d**) IVM of ILNs from CD11c-eYFP mice (DCs 'pseudocolored' green) given 1.5×10^7 OT-I cells ('pseudocolored' blue) and infected with VV-OVA (nonfluorescent construct encoding SIINFEKL) and then, 8–10 h after infection, given fluorescent dextran subcutaneously to label macrophages (red); images obtained 30 min later are presented as three-dimensional reconstructions of a 40-μm section. Scale bars, μm. All experiments were repeated at least two independent times.

lymph node were macrophages, as determined by their expression of the CD169 marker in cryosections (**Fig. 6a**). We also found that VSV infected mainly CD169$^+$ cells at the node periphery. To identify macrophages by IVM, we administered fluorescent-dextran by subcutaneous injection into mice infected with VV-OVA or VSV-OVA (nonfluorescent viruses expressing full-length ovalbumin) and analyzed OT-I cells (**Fig. 6b,c**). OT-I cells failed to cluster around dextran-positive macrophages after infection, 'preferentially' clustering in areas just lateral to or beneath the macrophage-rich zone (**Fig. 6b,c**). A subsequent experiment with mice expressing enhanced yellow fluorescent protein (eYFP) under control of the CD11c promoter (CD11c-eYFP mice), for visualization of DCs[25], showed that after infection with VV-OVA, OT-I cells nucleated around DCs (**Fig. 6d**). DCs are poorly labeled with dextran, which allowed us to distinguish DCs and macrophages.

We next used IVM to characterize the interaction of OT-I cells with YFP$^+$ DCs in the presence or absence of cognate antigen (**Fig. 7**). After infection with VV expressing antigen (VV-OVA), we detected many clusters of OT-I cells with DCs (**Fig. 7c** and **Supplementary Video 10** online). After infection with VV lacking cognate peptide (irrelevant VV), we detected more OT-I cell contacts with DCs than in uninfected mice (**Fig. 7a** versus **7b**) but did not detect the large clusters induced by virus expressing cognate antigen. As with VV-OVA, we identified many clusters between OT-I cells and DCs in ILNs infected with VSV-OVA (expressing SIINFEKL; **Fig. 7d**).

To quantify the requirement for cognate antigen for DC contact after viral infection, we counted T cells and DCs after infection with antigen-bearing or irrelevant virus (**Fig. 7e,f** and **Supplementary Video 9**). After transferring OT-I cells into CD11c-eYFP mice and then infecting them with virus, we obtained a series of high-magnification images of the peri-SCS area of the lymph node (each covering 40 μm in depth) and counted OT-I cells per DC in five fields per experiment. After infection with irrelevant VV, we detected a slightly more DCs contacting a single OT-I cell than in uninfected controls (result not statistically significant). Notably, after infection with VV-OVA or VSV-OVA, we detected many DCs interacting with over ten OT-I cells, and in some cases found 20 CD8$^+$ T cells clustering with a single DC (**Fig. 7f**, top). The average number of T cells per DC was significantly enhanced in the presence of cognate antigen: 1.35 ± 0.11 versus 5.69 ± 0.61 for irrelevant VV versus VV-OVA; 1.44 ± 0.24 versus 4.79 ± 0.39 for irrelevant VSV versus VSV-OVA (mean ± s.e.m.; **Fig. 7f**, bottom). These data collectively indicate that DCs located at the periphery of the lymph node serve as the initial APCs after infection with lymph-borne virus.

Full CD8$^+$ T cell activation in the first 12 h after infection

Next we addressed two critical questions. Does the formation of clusters of OT-I cells and APCs at the periphery result in OT-I T cell activation, and do cells activated in the first 12 h after infection become important antiviral effectors? To maximize the fraction of activated OT-I cells, we labeled cells with the cytosolic dye CFSE, transferred only 1×10^6 CFSE-labeled cells and determined activation by *ex vivo* flow cytometry of expression of the early CD8$^+$ T cell activation marker CD69 (**Fig. 8a**). At 12 h after infection with VV-NP-S-eGFP, 42% of OT-I cells recovered from the ILN had upregulated CD69. To determine the precise location of OT-I cell activation, whether deeper in the T cell zone or in or near clusters in the ILN periphery, we explanted ILN 12 h after infection with VV-NP-S-eGFP and stained live-tissue vibratome sections with monoclonal antibody to CD69. In agreement with our IVM observations, we found antigen-specific OT-I cells clustered with VV-infected cells (**Fig. 8b**). Clustered OT-I cells had surface expression of CD69, whereas most unclustered OT-I cells (many OT-I cells were not involved in conjugates) had low and/or undetectable CD69 expression. Therefore, activation of antigen-specific CD8$^+$ T cells can occur during the formation of clusters with infected APCs in the node periphery.

To better characterize CD8$^+$ T cell activation in the lymph node within the first 12 h after infection, we used anti-CD62L to block the entry of OT-I cells at increasing intervals after infection. As reported before[9], intravenous injection of 100 μg of blocking antibody substantially decreased the number of OT-I cells trafficking into even heavily infected nodes (**Fig. 8c**). For these studies, we used cervical lymph nodes, which have a more defined pattern of lymph drainage than do ILNs but have a pattern of OT-I cell relocation after infection

nearly identical to that of ILNs. Notably, there were no substantial differences in the amount of OT-I cell proliferation, granzyme B staining or interferon-γ production when cells were allowed to enter the lymph node for only 12 h after infection (**Fig. 8d**), which indicated that early events were sufficient for full activation of OT-I cells.

Do CD8$^+$ T cells activated during the first 12 h after infection traffic to the peripheral infection site? To assess this, we infected one ear by intradermal injection to create a local nidus of VV infection and blocked OT-I lymph node entry at various intervals with anti-CD62L. At 4 d after infection, we removed and dissociated infected ears and quantified the OT-I cells present by flow cytometry. Treatment with anti-CD62L before OT-I cell transfer reduced aural OT-I cells significantly, which demonstrated the efficacy of the treatment. Notably, antibody administered at 0 h after infection had only a slight effect on the trafficking of OT-I cells to the inflamed ear and had no effect when delayed to 12 h after infection (**Fig. 8e**).

DISCUSSION

We have shown here that in lymph nodes collecting lymph borne-virus, CD8$^+$ T cells interacted with virus-infected cells just below the lymph node SCS, an area we call the 'peripheral interfollicular region'. This region is an important site, and possibly the principal site, for the initial encounter of lymph-borne viruses and naive lymphocytes. Previous studies of DC-lymphocyte interactions in the lymph node, which described priming of B lymphocytes and T lymphocytes in a deeper area of the lymph node adjacent to HEVs, used either adoptively transferred antigen-pulsed DCs or soluble antigens administered with microbial adjuvants to enhance immunogenicity[7,9,20,21,26]. Transferred DCs initially localize to paracortical regions in close proximity to HEVs before gradually incorporating into the lymph node DC network[7,9,25]. Although such conditions relate to some vaccination strategies, they poorly mimic immune responses to viruses and other particulate antigens and pathogens. Using IVM after virus

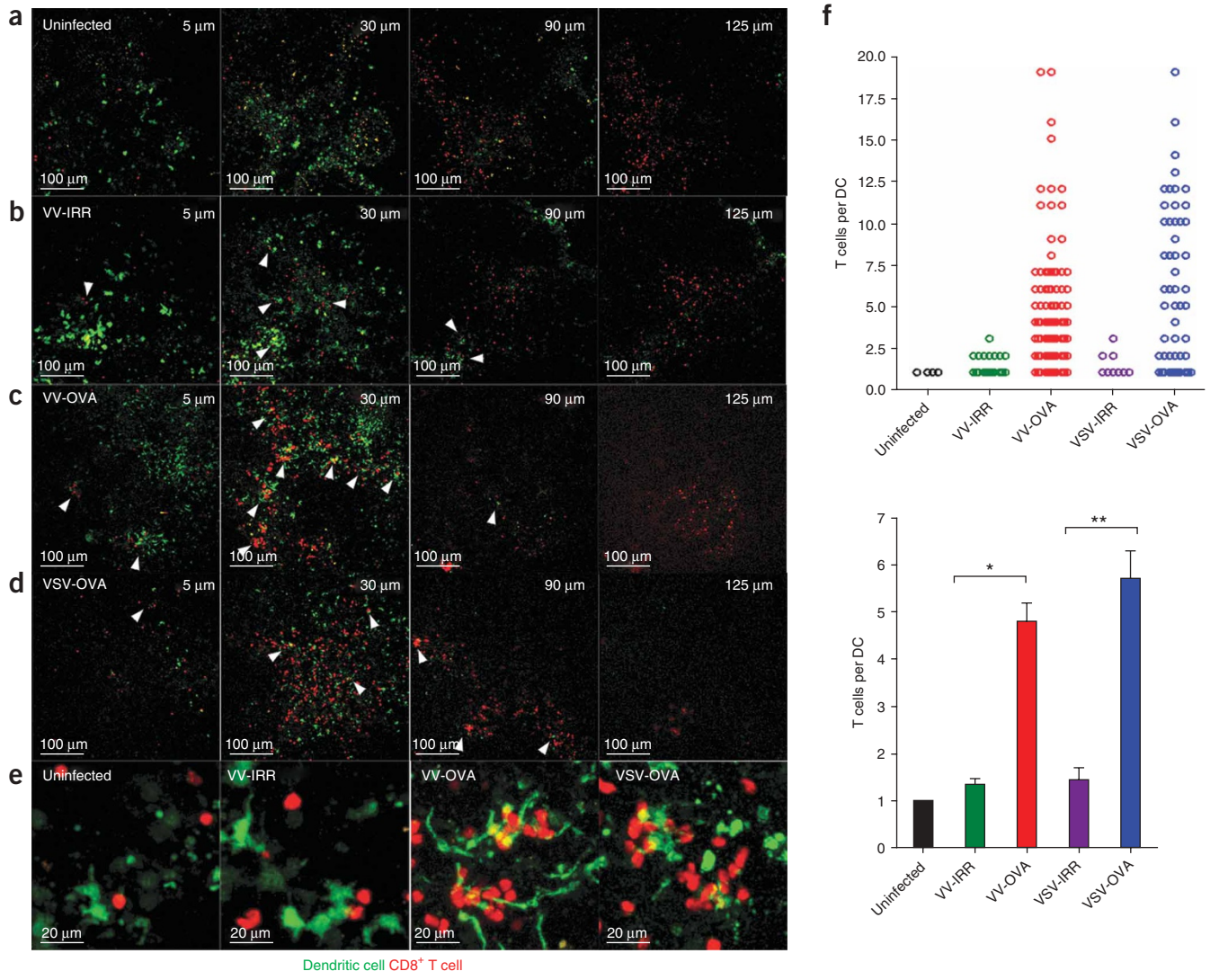

Figure 7 CD8$^+$ T cells interact with DCs under the SCS. (**a**–**d**) IVM of ILNs from CD11c-eYFP mice (DCs 'pseudocolored' green) given 1.5×10^7 OT-I cells (red) before infection with nonfluorescent virus; images obtained 6–12 h after infection are presented as individual 5-μm sections obtained at a depth of 5, 30, 90 or 125 μm beneath the ILN surface. White arrowheads indicate CD8$^+$ T cells interacting with DCs. VV-OVA and VSV-OVA encode SIINFEKL; VV-IRR is irrelevant VV lacking cognate peptide. (**e**) Higher-magnification views of OT-I cell–DC interactions in **a**–**d** (infecting virus, top left corner). (**f**) Dendritic cells and OT-I cells in five IVM fields for each condition (virus-infected or uninfected, plotted as OT-I cells/individual DC (top) or average number of OT-I cells/DCs (bottom). *, $P < 0.001$; **, $P = 0.001$ (unpaired *t*-test). All experiments were repeated at least two independent times.

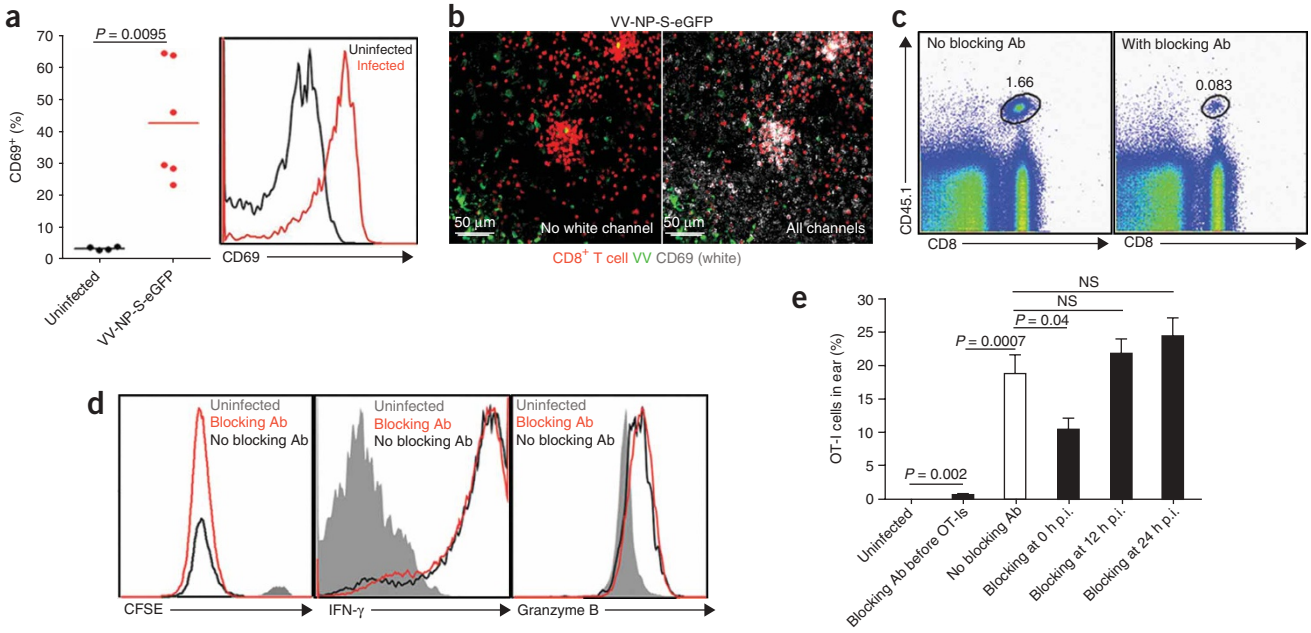

Figure 8 Early interactions with VV-infected cells activate OT-I cells. (**a**) Flow cytometry of expression of the early activation marker CD69 in OT-I cells in lymph nodes from mice given 1×10^6 CFSE-labeled OT-I cells 12 h before being infected with VV-NP-S-eGFP, analyzed 12 h after infection. Each dot (left) represents an individual node; horizontal lines indicate mean. (**b**) CD69 staining of live sections of ILNs removed 12 h after infection with VV-NP-S-eGFP: red, OT-I cells; green, infected cells. Right, CD69 staining overlaid in white. (**c**) Flow cytometry of OT-I cells ($CD45.1^+$ $CD8^+$ cells) entering a VV-infected lymph node without (left) and with (right) treatment with monoclonal anti-CD62L (blocking Ab); lymph nodes were analyzed 12 h after infection. (**d**) Flow cytometry of cervical lymph nodes from mice given 2×10^6 OT-I cells, then infected intradermally in the ear with 1×10^6 PFU of VV-NP-S-eGFP and left untreated (black lines) or treated with 100 μg monoclonal anti-CD62L at 12 h after infection (red lines), analyzed 48 h after infection. Gray filled histograms, OT-I cells from uninfected mice. Left, CFSE dilution; middle and right, intracellular staining for IFN-γ (middle) or granzyme B (right). (**e**) Peripheral trafficking of activated $CD8^+$ T cells in mice given 2×10^6 OT-I cells, then left uninfected or infected intradermally in the ear with 1×10^6 PFU of VV-NP-S-eGFP; mice received anti-CD62L before the addition of OT-I cells (OT-Is) or at 0, 12 or 24 h after infection (p.i.; filled bars), or did not receive anti-CD62L (open bar), and ears were analyzed 4 d after infection. Each bar represents the average of four ears. Statistical analyses, unpaired *t*-test; NS, not significant. Each experiment was repeated two to four times independently.

infection with two widely divergent viruses, we have made many observations here that are probably more applicable to understanding the general principles of the activation of antiviral immune responses in peripheral lymph nodes.

First, after viral infection, $CD8^+$ T cell priming occurred in a thin, nearly sessile layer just beneath the SCS. SCS macrophages form a nonmotile layer of cells that often penetrate the SCS lining cells, thereby gaining access to lymph deposited in the sinus[12,27,28]. SCS macrophages have been shown to acquire many particulate antigens, including inactivated VSV virions, and deliver them to follicular B cells[29]. A notable feature of these macrophages is their ability to retain antigenic complexes on their surface for capture by follicular B cells, which has been suggested to result from limited phagocytic capacity or from rapid recycling between endosomes and the cell surface[12]. Because these macrophages are heavily infected by lymph-borne virus, it will be useful to determine if infection results from a relatively rare internalization event when the macrophage surface is coated with virions or if these poorly phagocytic cells are actually adept at endocytosing incoming virions. One possibility is that macrophages and DCs in the peripheral interfollicular region sample the SCS for incoming virions with the 'goal' of becoming infected for direct presentation to $CD8^+$ T cells. The handling of particulate antigens in the lymph node by SCS macrophages may contribute to the enhanced ability of such antigens to induce $CD8^+$ T cell responses[30].

Second, we have shown that redistribution of $CD8^+$ T cells in response to viral infection was mostly but not entirely antigen specific. In the absence of cognate peptide but in the presence of MHC class I molecules, we consistently noted a slightly higher density of OT-I cells at the lymph node periphery. This suggests that virus induction induces the migration of $CD8^+$ T cells to the periphery and that $CD8^+$ T cell accumulation is based on the strength of interaction with infected cells, which we have shown governs the length of contact between $CD8^+$ T cells and infected DCs. However, we cannot exclude the possibility of a contribution from antigen-specific recruitment of $CD8^+$ T cells to the peripheral interfollicular region. This could result from the extension of very thin dendrites from infected cells into the node interior that guide $CD8^+$ T cells to the cell body. It is also conceivable that $CD8^+$ T cells follow an antigen gradient created by peptide diffusion between cells with gap junctions[31].

Third, we have shown that after infection by lymph-borne virus, $CD8^+$ T cells interacted specifically with DCs located just outside the macrophage-rich zone of the lymph node. In the conditions we used, up to 20 $CD8^+$ T cells contacted a single DC in a peptide-dependent way. The slowing of $CD8^+$ T cells in the peripheral interfollicular region was the direct result of their interaction with APCs and was not due simply due to physical constraints on motion, as suggested before[32]. We have shown that stable contacts between antigen-specific $CD8^+$ T cells and virus-infected DCs were formed much more rapidly than reported before for phase II (stable) interactions between $CD8^+$ T cells and peptide-pulsed, adoptively transferred DCs[9]. Notably, with VV and VSV, such contacts can initiate within minutes of the entry of T cells into an infected-cell region and are maintained even in the

presence of large numbers of competing T cells. As the duration of these interactions are controlled by the amount of peptide-MHC complexes on the APC surface[33], this suggests that direct priming in the conditions we used rapidly generated sufficient quantities of peptide to enable phase II contacts. For comparison, bypass of phase I contacts with DCs pulsed with synthetic peptides requires peptide concentrations of over 1 μM (refs. 9,21; data not shown), which generates thousands to tens of thousands of cell surface complexes[34].

Fourth, we have provided IVM evidence that $CD8^+$ T cells were activated by interaction with VSV- and VV-infected cells (through direct priming). Activation resulted from encounters between $CD8^+$ T cells and DCs that could have been initiated throughout the entire period (2 d) that infected cells were detected in the lymph node. *In vivo* ablation studies at various times after transfer of peptide-pulsed DCs have established that brief periods of antigenic stimulation are sufficient for generating $CD8^+$ T cells effectors[35]. Extending those findings to viral infection, we have shown that interactions occuring in the lymph node in the first 12 h after infection resulted in $CD8^+$ T cell activation indistinguishable phenotypically from activation occurring at later times in the lymph node. We have established that such 'first-responder' $CD8^+$ T cells rapidly trafficked back to the site of viral challenge. These data suggest that for many viral infections, $CD8^+$ T cells primed in the peripheral interfollicular region soon after viral infection of the lymph node represent effector cells for controlling events at the initial infection site. Although in natural conditions there are many fewer naive $CD8^+$ T cells than even the lowest numbers of OT-I cells we adoptively transferred here, there could still be a sufficient number of activated cells to exert a potent antiviral effect, particularly if there are relatively few infected cells at the primary infection site.

There may be important additional functional consequences for the initial wave of viral antigen presentation in the lymph node. It has been reported that the fate of activated T cells could be greatly influenced by their time of arrival in the lymph node after immunization with soluble antigen[36]. Such a functional dichotomy may be particularly important during even acute viral infection, when prolonged antigen presentation is often the rule[37–39]. Although divergent $CD4^+$ T cell memory phenotypes were attributed previously to increased antigen density during the second wave of nodal antigen presentation[36], our study raises the possibility that priming at a distinct location in the node may function to shape the differential profiles of memory cells encountered after viral infection. Future IVM studies should determine how the particular features of different viruses and different antigens influence events in the lymph node leading to immune activation. It is likely that the outcome is influenced, perhaps greatly, by viral activation of innate immune cells (such as natural killer cells and plasmacytoid DCs) and the tactics viruses use to minimize immune interference with their evolutionary imperative to maximize transmission between hosts.

METHODS

Animals and injections. Specific pathogen–free C57BL/6NTac mice (wild-type), C57BL/6-[KO]H-$2K^b$-[KO]H-$2D^b$ mice (H-$2K^b$H-$2D^b$ deficient), B6(Ly5.1)-[Tg]OT-I-[KO]RAG1 mice (OT-I) and C57BL/6-[Tg]CD11c:EYFP mice (expressing eYFP under control of the CD11c promoter) were from Taconic Farms; B6.FVB-Tg(Itgax-DTR/EGFP)57Lan/J mice (expressing eGFP under control of the CD11c promoter) were from Jackson Laboratories. For *in vivo* infection, mice were given approximately 3.5×10^7 plaque-forming units (PFU) of VV or 4.0×10^7 PFU of VSV subcutaneously in ten injections near the hindlimb-torso transition. Most images were acquired during the period 4–12 h after injection (specific time in figures and legends). All procedures involving animals were approved by the Animal Care and Use Committee of the National Institute of Allergy and Infectious Diseases.

Viruses. VVs used in this study were generated as described[40]. VV expressing influenza virus nucleoprotein from the A/Puerto Rico/8/34 strain of influenza virus fused to chicken ovalbumin peptide (amino acids 257–264) followed by a carboxy-terminal fusion to eGFP (VV-NP-S-eGFP) has been described[14]. Other VVs used in this study were VV-eGFP (lacking SIINFEKL), VV-OVA (non-fluorescent construct expressing SIINFEKL) and VV-NT60 NP (nonfluorescent construct expressing influenza A virus nucleoprotein from the A/NT/60/68 strain of influenza virus). VSV expressing the same constructs was generated as described[41].

Imaging reagents. For visualization of the SCS, 33 μg FITC- or rhodamine-conjugated wheat germ agglutinin (Invitrogen) was injected (in the same way as virus) 30 min before imaging of the ILN. For visualization of blood vessels, approximately 0.5 mg fluorescein-conjugated dextran (500 kilodaltons; Invitrogen) was injected intravenously. For visualization of macrophages, mice were given 0.2 mg fluorescein- or rhodamine-conjugated dextran subcutaneously (70 kilodaltons). For imaging of HEVs, approximately 250 μl FITC-conjugated HEV-specific monoclonal antibody (MECA-79; Santa Cruz Biotechnology) was injected intravenously 10–15 min before imaging. For blockade of the entry of $CD8^+$ T cells to the lymph node through HEVs (as described[9]), 100 μg monoclonal anti-CD62L (Mel-14; American Type Culture Collection) was given at various times.

Two-photon microscopy. $CD8^+$ T cells (5×10^6 to 2×10^7; number provided in figure legend) labeled with CFSE (carboxyfluorescein succinimidyl ester), CMTPX ($C_{42}H_{40}ClN_3O_4$) or CMF_2HC (4-chloromethyl-6,8-difluoro-7-hydroxycoumarin; all from Invitrogen) were injected intravenously 12–24 h before injection with virus, unless specified otherwise. Two-photon imaging used an inverted Leica TCS-SP2 MP confocal microscope (Leica Microsystems) equipped with a 20× objective (numerical aperture, 0.7) or 63× objective (numerical aperture, 1.30) and with 80% glycerol as the immersion medium for each objective. Two-photon excitation was provided by a Mai Tai Ti:Sapphire laser (Spectra Physics) with a 10-Watt pump, tuned to 800 nm for imaging of cells labeled with CMTPX, FITC or CMF_2HC; 850 nm for imaging of cells labeled with CMTPX in combination with eGFP; or 900 nm for imaging of eGFP alone or for imaging of second-harmonic generation. Emitted fluorescence was collected with a two-channel non-descanned detector. Wavelength separation was accomplished with a dichroic mirror at 560 nm followed by emission filters of 525/50 nm bendpass and 610/75 nm bendpass. For four-dimensional analysis of cell migration, the 20× objective was used to obtain stacks of 34 sections (z step = 5 μm) acquired every 1 min to provide an imaging volume 165 μm in depth. For imaging of cellular interactions, the 63× objective was used and stacks of 25 sections obtained with a 2.5-μm z-step for a total depth of 40–60 μm were obtained every 1–2 min.

Data analysis. Data were analyzed with an Imarisx64 v5.03 (Bitplane). Images were first processed with the Gaussian filter algorithm. Average speeds calculated with the spot-detection function and the following parameters: autoregressive motion gapclose 3 algorithm, 7.5-μm object diameter and 40-μm maximum distance (every 60 s). Cells were excluded unless they remained in the viewing area for 5 min or more. For calculation of cell numbers at increasing depths under the SCS, the maximum number of cells in any one section was used as the denominator (number of cells per section/maximum number of cells in any section) because of the much higher number of $CD8^+$ T cells in the ILN after viral infection. For calculation of the number of $CD8^+$ T cells per DC, five fields (239 μm × 239 μm × 40 μm) were acquired in a given infected and/or uninfected ILN at high magnification (×63) and the number of $CD8^+$ T cells per DC was summed in all five fields. Groups were analyzed for statistical significance with an unpaired t-test; error bars represent s.e.m.

Immunohistochemistry. ILNs were removed at 12 h after infection and were rapidly frozen in optimum cutting temperature compound (Electron Microscopy Sciences), and 30-μm cryosections were cut. Individual sections were thawed, were fixed for 20 min with 3.2% (vol/vol) paraformaldehyde in

10% (wt/vol) sucrose, and were stained with FITC-conjugated HEV-specific monoclonal antibody (MECA-79; BD Biosciences) followed by indodicarbocyanine-conjugated goat anti-rat IgM (112-176-075; Jackson ImmunoResearch). Serial images of a single lymph node cross-section were acquired and were reconstructed into a complete lymph node with Imarisx64 v5.03 and Adobe Photoshop (Apple). For detection of CD69 in live-tissue sections, ILNs were removed 12 h after infection with VV-NP-S-eGFP and were embedded into 1% (wt/vol) agarose (SeaKem LE; Biowhittaker Molecular Applications). ILNs were cut into sections 250 μm in thickness with a vibrating-blade microtome (T 1000S; Leica Microsystems) and were stained for 3–5 h at 4 °C with hamster anti-CD69 (H1.2F3; AbD Serotec) followed by incubation for 2 h at 4 °C with indodicarbocyanine-conjugated anti-hamster (127-175-160; Jackson Immunoresearch). Stained sections (live or fixed) were examined by confocal microscopy (TCS-SP5 DMI6000; Leica Microsystems). Basement membranes were visualized on frozen sections by staining with anti-perlecan (heparan sulfate proteoglycan 2; A7L6; Abcam) followed by Alexa Fluor 647–conjugated goat anti-rat (A-21247; Invitrogen). $CD169^+$ macrophages were visualized on frozen sections by staining with anti-CD169 (ED3; AbD Serotec) followed by Alexa Fluor 647–conjugated goat anti-rat (A-21247, Invitrogen).

T cell activation analysis. OT-I cells were labeled for 10 min at 37 °C with 7.5 μM CFSE (Invitrogen) in PBS plus 0.1% (wt/vol) BSA, and 1×10^6 cells were transferred intravenously into uninfected mice. Then, 12 h later, mice were given VV-NP-S-eGFP. ILNs were removed at 12 h after infection and stained for CD69 (H1.2F3) and CD25 (PC61; both from BD Biosciences). Cells were analyzed on an LSRII flow cytometer (BDBiosciences) and data were analyzed with FlowJo software (TreeStar).

For analysis of the properties of $CD8^+$ T cells present in the lymph node at the time of infection or recruitment to the ear, mice were given 2×10^6 OT-I cells and, 12 h after cell transfer, were infected in the ear with 1.0×10^6 PFU of VV-NP-S-eGFP. Anti-CD62L (Mel-1t; American Type Culture Collection) was administered at 12 h after infection unless otherwise indicated. At 48 h after infection, draining cervical lymph nodes were removed and OT-I cells were gated with anti-CD8 (53-6.7) and anti-CD45.1 (A20; both from BD Biosciences) and then analyzed for CFSE dilution. For analysis of interferon-γ production, cells were restimulated with SIINFEKL *in vitro* for 4 h after infection before intracellular staining. Cells were analyzed directly *ex vivo* for production of intracellular granzyme B (16G6; eBioscience). Ears were removed at day 4 after infection and single-cell suspensions were analyzed by flow cytometry for the percentage of transferred OT-I cells ($CD8^+$, $CD45.1^+$).

Note: Supplementary information is available on the Nature Immunology website.

ACKNOWLEDGMENTS

We thank O. Schwartz, M. Czapiga, J. Kabat and S. Han for imaging advice and insight; D. Tokarchick and K. Irvine for technical assistance; and the staff of the Comparative Medical Branch of the National Institute of Allergy and Infectious Diseases (building 33) for animal care. Supported by the Intramural Research Program of National Institute of Allergy and Infectious Diseases.

AUTHOR CONTRIBUTIONS

H.D.H., J.W.Y. and J.R.B. conceptualized and designed the research; H.D.H. did the IVM experiments and analyzed data; K.T. did the sectioning experiments (live and frozen); C.N.S. and F.R.M. prepared mice for IVM and aided in flow cytometry experiments; S.E.H. did lymph flow experiments; J.L. and G.N.B. generated recombinant VSVs; and H.D.H., J.R.B. and J.W.Y. prepared the manuscript.

Published online at http://www.nature.com/natureimmunology
Reprints and permissions information is available online at http://npg.nature.com/reprintsandpermissions

1. Gretz, J.E., Norbury, C.C., Anderson, A.O., Proudfoot, A.E. & Shaw, S. Lymph-borne chemokines and other low molecular weight molecules reach high endothelial venules via specialized conduits while a functional barrier limits access to the lymphocyte microenvironments in lymph node cortex. *J. Exp. Med.* **192**, 1425–1440 (2000).
2. Sixt, M. *et al.* The conduit system transports soluble antigens from the afferent lymph to resident dendritic cells in the T cell area of the lymph node. *Immunity* **22**, 19–29 (2005).
3. Halin, C., Rodrigo Mora, J., Sumen, C. & von Andrian, U.H. In vivo imaging of lymphocyte trafficking. *Annu. Rev. Cell Dev. Biol.* **21**, 581–603 (2005).
4. Bajenoff, M. *et al.* Highways, byways and breadcrumbs: directing lymphocyte traffic in the lymph node. *Trends Immunol.* **28**, 346–352 (2007).
5. Germain, R.N., Miller, M.J., Dustin, M.L. & Nussenzweig, M.C. Dynamic imaging of the immune system: progress, pitfalls and promise. *Nat. Rev. Immunol.* **6**, 497–507 (2006).
6. Cahalan, M.D. & Parker, I. Imaging the choreography of lymphocyte trafficking and the immune response. *Curr. Opin. Immunol.* **18**, 476–482 (2006).
7. Bousso, P. & Robey, E. Dynamics of $CD8^+$ T cell priming by dendritic cells in intact lymph nodes. *Nat. Immunol.* **4**, 579–585 (2003).
8. Miller, M.J., Wei, S.H., Cahalan, M.D. & Parker, I. Autonomous T cell trafficking examined in vivo with intravital two-photon microscopy. *Proc. Natl. Acad. Sci. USA* **100**, 2604–2609 (2003).
9. Mempel, T.R., Henrickson, S.E. & Von Andrian, U.H. T-cell priming by dendritic cells in lymph nodes occurs in three distinct phases. *Nature* **427**, 154–159 (2004).
10. Qi, H., Egen, J.G., Huang, A.Y. & Germain, R.N. Extrafollicular activation of lymph node B cells by antigen-bearing dendritic cells. *Science* **312**, 1672–1676 (2006).
11. Pape, K.A., Catron, D.M., Itano, A.A. & Jenkins, M.K. The humoral immune response is initiated in lymph nodes by B cells that acquire soluble antigen directly in the follicles. *Immunity* **26**, 491–502 (2007).
12. Phan, T.G., Grigorova, I., Okada, T. & Cyster, J.G. Subcapsular encounter and complement-dependent transport of immune complexes by lymph node B cells. *Nat. Immunol.* **8**, 992–1000 (2007).
13. Carrasco, Y.R. & Batista, F.D. B cells acquire particulate antigen in a macrophage-rich area at the boundary between the follicle and the subcapsular sinus of the lymph node. *Immunity* **27**, 160–171 (2007).
14. Norbury, C.C., Malide, D., Gibbs, J.S., Bennink, J.R. & Yewdell, J.W. Visualizing priming of virus-specific $CD8^+$ T cells by infected dendritic cells *in vivo*. *Nat. Immunol.* **3**, 265–271 (2002).
15. Wei, S.H. *et al.* Sphingosine 1-phosphate type 1 receptor agonism inhibits transendothelial migration of medullary T cells to lymphatic sinuses. *Nat. Immunol.* **6**, 1228–1235 (2005).
16. Katakai, T. *et al.* A novel reticular stromal structure in lymph node cortex: an immunoplatform for interactions among dendritic cells, T cells and B cells. *Int. Immunol.* **16**, 1133–1142 (2004).
17. Bajenoff, M., Granjeaud, S. & Guerder, S. The strategy of T cell antigen-presenting cell encounter in antigen-draining lymph nodes revealed by imaging of initial T cell activation. *J. Exp. Med.* **198**, 715–724 (2003).
18. Allan, R.S. *et al.* Epidermal viral immunity induced by $CD8\alpha^+$ dendritic cells but not by Langerhans cells. *Science* **301**, 1925–1928 (2003).
19. Belz, G.T. *et al.* Cutting edge: conventional $CD8\alpha^+$ dendritic cells are generally involved in priming CTL immunity to viruses. *J. Immunol.* **172**, 1996–2000 (2004).
20. Miller, M.J., Safrina, O., Parker, I. & Cahalan, M.D. Imaging the single cell dynamics of $CD4^+$ T cell activation by dendritic cells in lymph nodes. *J. Exp. Med.* **200**, 847–856 (2004).
21. Miller, M.J., Hejazi, A.S., Wei, S.H., Cahalan, M.D. & Parker, I. T cell repertoire scanning is promoted by dynamic dendritic cell behavior and random T cell motility in the lymph node. *Proc. Natl. Acad. Sci. USA* **101**, 998–1003 (2004).
22. Bajenoff, M. *et al.* Stromal cell networks regulate lymphocyte entry, migration, and territoriality in lymph nodes. *Immunity* **25**, 989–1001 (2006).
23. Miller, M.J., Wei, S.H., Parker, I. & Cahalan, M.D. Two-photon imaging of lymphocyte motility and antigen response in intact lymph node. *Science* **296**, 1869–1873 (2002).
24. Hendriks, H.R., Duijvestijn, A.M. & Kraal, G. Rapid decrease in lymphocyte adherence to high endothelial venules in lymph nodes deprived of afferent lymphatic vessels. *Eur. J. Immunol.* **17**, 1691–1695 (1987).
25. Lindquist, R.L. *et al.* Visualizing dendritic cell networks *in vivo*. *Nat. Immunol.* **5**, 1243–1250 (2004).
26. Castellino, F. *et al.* Chemokines enhance immunity by guiding naive $CD8^+$ T cells to sites of $CD4^+$ T cell-dendritic cell interaction. *Nature* **440**, 890–895 (2006).
27. Farr, A.G., Cho, Y. & De Bruyn, P.P. The structure of the sinus wall of the lymph node relative to its endocytic properties and transmural cell passage. *Am. J. Anat.* **157**, 265–284 (1980).
28. Fossum, S. The architecture of rat lymph nodes. II. Lymph node compartments. *Scand. J. Immunol.* **12**, 411–420 (1980).
29. Junt, T. *et al.* Subcapsular sinus macrophages in lymph nodes clear lymph-borne viruses and present them to antiviral B cells. *Nature* **450**, 110–114 (2007).
30. Yewdell, J.W., Norbury, C.C. & Bennink, J.R. Mechanisms of exogenous antigen presentation by MHC class I molecules in vitro and in vivo: implications for generating $CD8^+$ T cell responses to infectious agents, tumors, transplants, and vaccines. *Adv. Immunol.* **73**, 1–77 (1999).
31. Neijssen, J. *et al.* Cross-presentation by intercellular peptide transfer through gap junctions. *Nature* **434**, 83–88 (2005).
32. Huang, A.Y., Qi, H. & Germain, R.N. Illuminating the landscape of in vivo immunity: insights from dynamic in situ imaging of secondary lymphoid tissues. *Immunity* **21**, 331–339 (2004).
33. Garcia, Z. *et al.* Competition for antigen determines the stability of T cell-dendritic cell nteractions during clonal expansion. *Proc. Natl. Acad. Sci. USA* **104**, 4553–4558 (2007).

34. Christinck, E.R., Luscher, M.A., Barber, B.H. & Williams, D.B. Peptide binding to class I MHC on living cells and quantitation of complexes required for CTL lysis. *Nature* **352**, 67–70 (1991).
35. Prlic, M., Hernandez-Hoyos, G. & Bevan, M.J. Duration of the initial TCR stimulus controls the magnitude but not functionality of the CD8$^+$ T cell response. *J. Exp. Med.* **203**, 2135–2143 (2006).
36. Catron, D.M., Rusch, L.K., Hataye, J., Itano, A.A. & Jenkins, M.K. CD4$^+$ T cells that enter the draining lymph nodes after antigen injection participate in the primary response and become central-memory cells. *J. Exp. Med.* **203**, 1045–1054 (2006).
37. Jelley-Gibbs, D.M. *et al.* Unexpected prolonged presentation of influenza antigens promotes CD4 T cell memory generation. *J. Exp. Med.* **202**, 697–706 (2005).
38. Zammit, D.J., Turner, D.L., Klonowski, K.D., Lefrancois, L. & Cauley, L.S. Residual antigen presentation after influenza virus infection affects CD8 T cell activation and migration. *Immunity* **24**, 439–449 (2006).
39. Turner, D.L., Cauley, L.S., Khanna, K.M. & Lefrancois, L. Persistent antigen presentation after acute vesicular stomatitis virus infection. *J. Virol.* **81**, 2039–2046 (2007).
40. Chakrabarti, S., Brechling, K. & Moss, B. Vaccinia virus expression vector: coexpression of β-galactosidase provides visual screening of recombinant virus plaques. *Mol. Cell. Biol.* **5**, 3403–3409 (1985).
41. Obuchi, M., Fernandez, M. & Barber, G.N. Development of recombinant vesicular stomatitis viruses that exploit defects in host defense to augment specific oncolytic activity. *J. Virol.* **77**, 8843–8856 (2003).